

Smad2 and Smad3 cooperate and antagonize simultaneously in vertebrate neurogenesis

David G. Míguez^{1,2,*}, Estel Gil-Guiñón¹, Sebastián Pons^{1,3} and Elisa Martí^{1,*}

¹Instituto de Biología Molecular de Barcelona, CSIC, C/Baldí i Reixac 20, Barcelona 08028, Spain

²Departamento de Física de la Materia Condensada and Instituto Nicolás Cabrera and IFIMAC, Universidad Autónoma de Madrid, Campus de Cantoblanco, 28046 Madrid, Spain

³Instituto de Investigaciones Biomédicas de Barcelona, CSIC-IDIBAPS, C/Roselló 161, Barcelona 08036, Spain

*Authors for correspondence (david.gomez.miguez@uam.es; emgbmc@ibmb.csic.es)

Accepted 4 September 2013

Journal of Cell Science 126, 5335–5343

© 2013. Published by The Company of Biologists Ltd

doi: 10.1242/jcs.130435

Summary

The transforming growth factor beta (TGF- β) pathway plays key roles in development and cancer. TGF- β signaling converges on the Smad2 and Smad3 effectors, which can either cooperate or antagonize to regulate their transcriptional targets. Here we performed *in vivo* and *in silico* experiments to study how such cooperativity and antagonism might function during neurogenesis. *In vivo* electroporation experiments in the chick embryo neural tube show that Smad2 and Smad3 cooperate to promote neurogenesis, as well as the transcription of Smad3-specific targets. Knockdown of Smad2 enhances neurogenesis and the transcription of Smad3-specific targets. A mathematical model of the TGF- β pathway fits the experimental results and predicts that the proportions of the three different trimeric complexes formed dictates the transcriptional responses of the R-Smad proteins. As such, Smad2 targets are activated solely by the Smad2–Smad2–Smad4 complex, whereas Smad3 targets are activated both by Smad2–Smad3–Smad4 and Smad3–Smad3–Smad4 trimers. We have modeled the Smad responses onto arbitrary genes and propose that this mechanism might be extended to additional activities of TGF- β in development and disease.

Key words: Neurogenesis, Neural tube, Differential equations, Chick embryo

Introduction

The transforming growth factor beta (TGF- β) pathway is one of the most conserved and prolific signaling cascades (Massagué, 2000; ten Dijke and Hill, 2004). Despite its simple architecture, this pathway is involved in the regulation of many processes, including growth, proliferation, differentiation and survival. Extracellular TGF- β and activin are ligands that bind to a type II transmembrane receptor, triggering the assembly of the tetrameric active ligand–receptor complex by binding to a type I receptor. Active ligand–receptor complexes then recruit and phosphorylate C-terminal residues of the downstream effectors Smad2 and Smad3 (R-Smad proteins). Phosphorylated R-Smad proteins form heterotrimeric complexes with Smad4 that enter the nuclei and recruit co-factors in order to ultimately regulate target gene expression (Fig. 1A–C) (Moustakas et al., 2001; Moustakas and Heldin, 2002). These DNA-binding complexes can contain two Smad2 and one Smad4 molecule (S224); two Smad3 and one Smad4 (S334); or even one Smad2, one Smad3 and one Smad4 molecule (S234) (Shi and Massagué, 2003).

Despite their 91% amino acid sequence similarity, Smad2 and Smad3 recruit different co-factors and target different regulatory sequences (Brown et al., 2007). However, they often share similar functions, playing redundant roles in ovarian granulosa cells (Li et al., 2008), in zebrafish mesoderm induction (Jia et al., 2008) and in other cellular contexts (Bernard, 2004). Moreover, when introduced into the *Smad2* locus, Smad3 can rescue the Smad2-deletion phenotype in developing mouse embryos (Dunn et al., 2005). However, Smad2 and Smad3 fulfil opposing roles in

breast cancer metastasis (Petersen et al., 2010) and regulation of growth and cell migration in pancreatic adenocarcinoma cells (Ungefroren et al., 2011), as well as in forkhead-dependent transcription (Labbé et al., 1998). Moreover, transcriptional profiling experiments showed that Smad3-activated genes are repressed by Smad2 (Yang et al., 2003). How such similar molecules can cooperate and/or antagonize distinct events remains somewhat unclear.

In this study, we characterized the roles of Smad2 and Smad3 in the context of vertebrate neurogenesis, where activation of the TGF- β pathway, in particular Smad3, has been shown to promote cell-cycle exit and differentiation (García-Campmany and Martí, 2007). Our results show a complex interplay between Smad2 and Smad3, where cooperation and antagonism occur simultaneously in the same cellular context. Through *in vivo* experiments in the chick embryo neural tube, we show that both knockdown and overexpression of Smad2 enhances neurogenesis. We developed a simplified mathematical model of the pathway in which all the experimental observations fit with a scenario in which neurogenesis is promoted by both S234 and S334 trimers.

Results and Discussion

Smad2 and Smad3 cooperate and act as antagonists in neurogenesis

To study the roles of Smad2 and Smad3 in the developing neural tube of the chick embryo *in vivo*, we first analyzed their expression in neural tube sections. Strong immunostaining for Smad2 and Smad3 was evident in the ventricular zone where

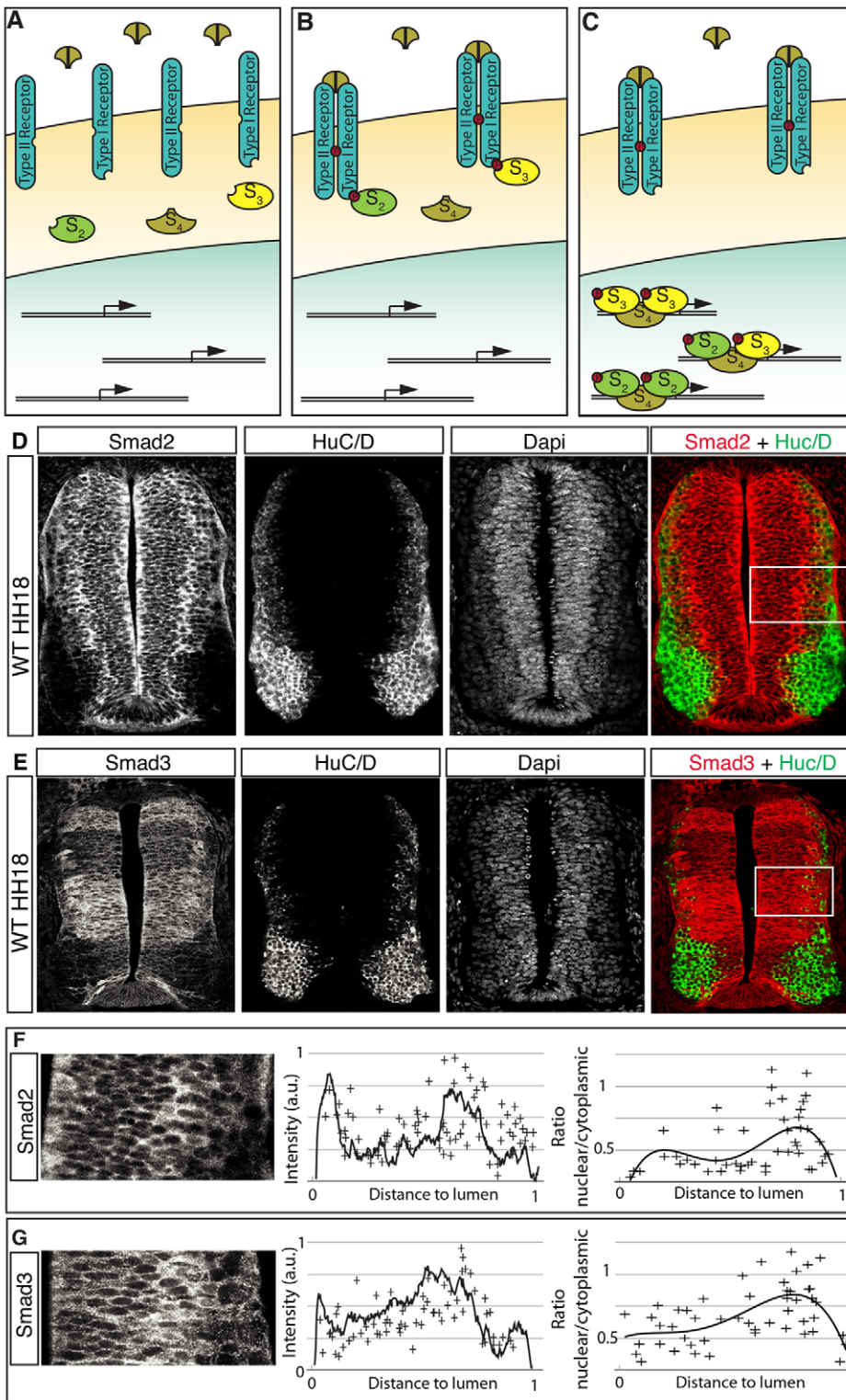


Fig. 1. Smad2 and Smad3 expression overlap in the developing neural tube.
(A–C) Scheme of the TGF- β pathway
(A) before, **(B)** during and **(C)** after ligand activation. S₂, Smad2; S₃, Smad3; S₄, Smad4.
(D,E) Selected sections co-immunostained for Smad2 and Smad3, the pan-neuronal marker HuC/D, and DAPI. **(D)** Smad2 expression throughout the ventricular zone. **(E)** Smad3 expression in restricted DV domains of the ventricular zone with no overlap with HuC/D (boxed areas show the regions selected for quantification). **(F,G)** Selected area for Smad2 and Smad3 quantification. Pixel intensity of Smad2 (**F**) and Smad3 (**G**) immunostaining versus distance to the lumen. Black lines correspond to the average profile and crosses correspond to single-cell values. Ratio of nuclear to cytoplasmic staining intensity versus distance to lumen for Smad2 (**F**) and Smad3 (**G**). Crosses correspond to single-cell measurements and lines correspond to polynomial fitting to illustrate the trend.

neural progenitors reside, with some enrichment in the transition zone (Fig. 1D,E). Although Smad2 is expressed throughout the dorsal–ventral (DV) axis of the neural tube (Fig. 1D), Smad3 expression is restricted to particular DV domains (Fig. 1E), as reported previously (Garcia-Campmany, 2007). Differentiated neurons that were identified by the expression of RNA-binding

proteins HuC and HuD (HuC/D) did not express Smad2 (Fig. 1D) or Smad3 (Fig. 1E), as confirmed by *in situ* hybridization, which showed the marginal zone of the neural tube where differentiated neurons reside to be devoid of Smad2 and Smad3 mRNA transcripts (supplementary material Fig. S1). To quantify Smad2 and Smad3 protein expression within the ventricular zone,

fluorescence intensity was measured at the intermediate neural tube (white rectangles in Fig. 1D,E) as a function of the distance to the lumen. Both total and single-cell measurements of Smad2 and Smad3 immunostaining intensity (black lines and crosses in Fig. 1F,G, respectively) indicated an enrichment in the transition zone. Moreover, single-cell measurements of the nuclear to cytoplasmic fluorescence intensity ratio as a function of distance to the lumen, showed that Smad2 and Smad3 are mainly located in the cytoplasm. However, as the nuclei move towards the transition zone, the average ratio of Smad2 and Smad3 within the nuclei increases (black lines in Fig. 1F,G, respectively), suggesting a potential transcriptional activation of Smad2 and Smad3 in the transition zone, where neurogenesis occurs.

Neurogenesis in the neural tube involves the lateral migration of neural progenitors committed to differentiation, as well as the *de novo* expression of pan-neural markers such as HuC/D. Thus, monitoring the position of electroporated cells by evaluating EGFP expression together with that of HuC/D serves to assess neurogenesis *in vivo* (Fig. 2A) (García-Campmany and Martí, 2007; Xie et al., 2011). When analyzed 48 hours post electroporation (hpe) of either control (pCIG) or Smad2, EGFP⁺ cells were evenly distributed throughout the ventricular zone and the mantle zone (HuC/D⁺ cells: Fig. 2E,F), although overexpression of Smad2 resulted in an increase in the total protein detected in western blots (Fig. 2B) and through the increased fluorescence intensity at the cellular level (Fig. 2C). However, Smad3 promoted the lateral migration of EGFP⁺ cells; a phenotype that was enhanced by the co-electroporation of Smad2 and Smad3 (Fig. 2G,H). When quantified, a significantly higher proportion of differentiated cells was detected after the electroporation of Smad3 and Smad2/3 (% GFP⁺, HuC/D⁺ cells at 48 hpe: 33±1% controls, 35±2% Smad2, 49±3% Smad3, 69±1% Smad2/3; Fig. 2I).

To test the requirement of Smad2/3 in neurogenesis, we reduced their endogenous expression by electroporating short-hairpin RNAs specific for chick Smad2 and Smad3. Electroporation of shSmad2 strongly diminished Smad2 protein expression (Fig. 2D,K), without affecting the endogenous expression of Smad3 (supplementary material Fig. S2). Conversely, electroporation of shSmad3 provoked a strong reduction in Smad3 protein expression (Fig. 2D,M), without affecting endogenous Smad2 expression (supplementary material Fig. S2). However, whereas knockdown of Smad3 caused the expected reduction in neurogenesis, knockdown of Smad2 resulted in a significant increase in neurogenesis (% GFP⁺, HuC/D⁺ cells at 48 hpe: 40±3% control, 63±3% shSmad2, 25±2% shSmad3; Fig. 2N). Together, these results suggest that Smad2 cooperates with Smad3 in the activation of target genes involved in neurogenesis, whereas it also antagonizes Smad3 activity in the same cellular context.

Smad2 and Smad3 cooperate and antagonize in Smad3-specific transcription

In order to dissect out the transcriptional responses mediated by Smad2 and Smad3, we expressed vectors containing luciferase reporters driven by either Smad2-specific [the activin response element (ARE)] (Chen et al., 1996) or Smad3-specific (-CAGA-) (Dennler et al., 1998) response elements (Fig. 3A–D) in the chick neural tube. The ARE reporter was activated 24 hpe of Smad2 in the chick neural tube, but not after Smad3 electroporation. However, co-electroporation of Smad3 with Smad2 interestingly

resulted in a strong decrease in ARE activity compared with that obtained with the same concentration of Smad2 alone (~3× reduction), reflecting antagonism between Smad2 and Smad3 in the regulation of the Smad2-specific targets (Fig. 3B). By contrast, the CAGA reporter was strongly activated by Smad3 but not by Smad2 electroporation. However, co-electroporation of Smad3 with Smad2 enhanced CAGA activity up to fivefold that of Smad3 alone, reflecting the cooperation between the Smad2 and Smad3 in the regulation of Smad3-specific targets (Fig. 3C).

Because knockdown of Smad2 resulted in increased neurogenesis, we assessed the transcriptional responses in the absence of either Smad2 or Smad3. The weak endogenous responses to the ARE reporter did not allow its activity to be monitored following loss of function, whereas knockdown of Smad3 (24 hpe of shSmad3) did reduce the activity of the CAGA reporter (Fig. 3D). Interestingly, knockdown of Smad2 resulted in strong activation (~20×) of the CAGA reporter (Fig. 3D). Because Smad3 expression levels were not increased after shSmad2 electroporation (supplementary material Fig. S2), these results suggest that the presence of Smad2 prevents Smad3 from activating its own targets, provoking an antagonistic effect.

To confirm these results at the cellular level, we co-electroporated Smad2 and Smad3 with the CAGA reporter driving EGFP expression (Fig. 3E–K). Although Smad2 was unable to activate CAGA-EGFP above control levels (Fig. 3E,F), Smad3 induced strong cell-autonomous activation of the reporter (Fig. 3G). Co-electroporation of Smad2 and Smad3 produced strong EGFP expression similar to that of Smad3 alone, which was probably due to saturation of EGFP expression (data not shown). Moreover, knockdown of Smad2, but not Smad3, induced cell-autonomous expression of CAGA-EGFP (Fig. 3H–K), which is consistent with the results from the luciferase experiments.

Mathematical model of the TGF-β pathway with differential activity predicts the dual cooperativity and antagonism of R-Smad proteins

The experimental data reflect a complex interplay between Smad2 and Smad3 in the regulation of their specific targets: a relationship that is reproduced in neurogenesis. In gain-of-function (GOF) experiments, Smad2 and Smad3 cooperate to regulate Smad3 targets and neurogenesis while antagonizing the regulation of Smad2-specific targets. Conversely, in loss-of-function (LOF) conditions Smad2 and Smad3 antagonize the regulation of Smad3-specific targets and neurogenesis. To understand the mechanisms driving such cellular responses, we developed a simplified theoretical model of the TGF-β pathway (see the Materials and Methods). Models have been developed previously to study nucleo-cytoplasmic shuttling (Clarke et al., 2006; Schmierer et al., 2008; Clarke and Liu, 2008), signal processing (Cellière et al., 2011), the generation of transient responses (Melke et al., 2006; Vilar et al., 2006; Zi et al., 2011) and the role of endocytosis (Zi and Klipp, 2007) in the TGF-β signaling pathway. However, to our knowledge, no model has been developed to predict how transcriptional responses are regulated.

We developed such a model that simulates the transcription of two arbitrary genes specific for Smad2 (Fig. 4A, black lines) and Smad3 (Fig. 4A, red lines). Increasing Smad2 levels (~7×, based on experimental data) enhances Smad2 target transcription (~7× increase) without significantly affecting direct Smad3 targets

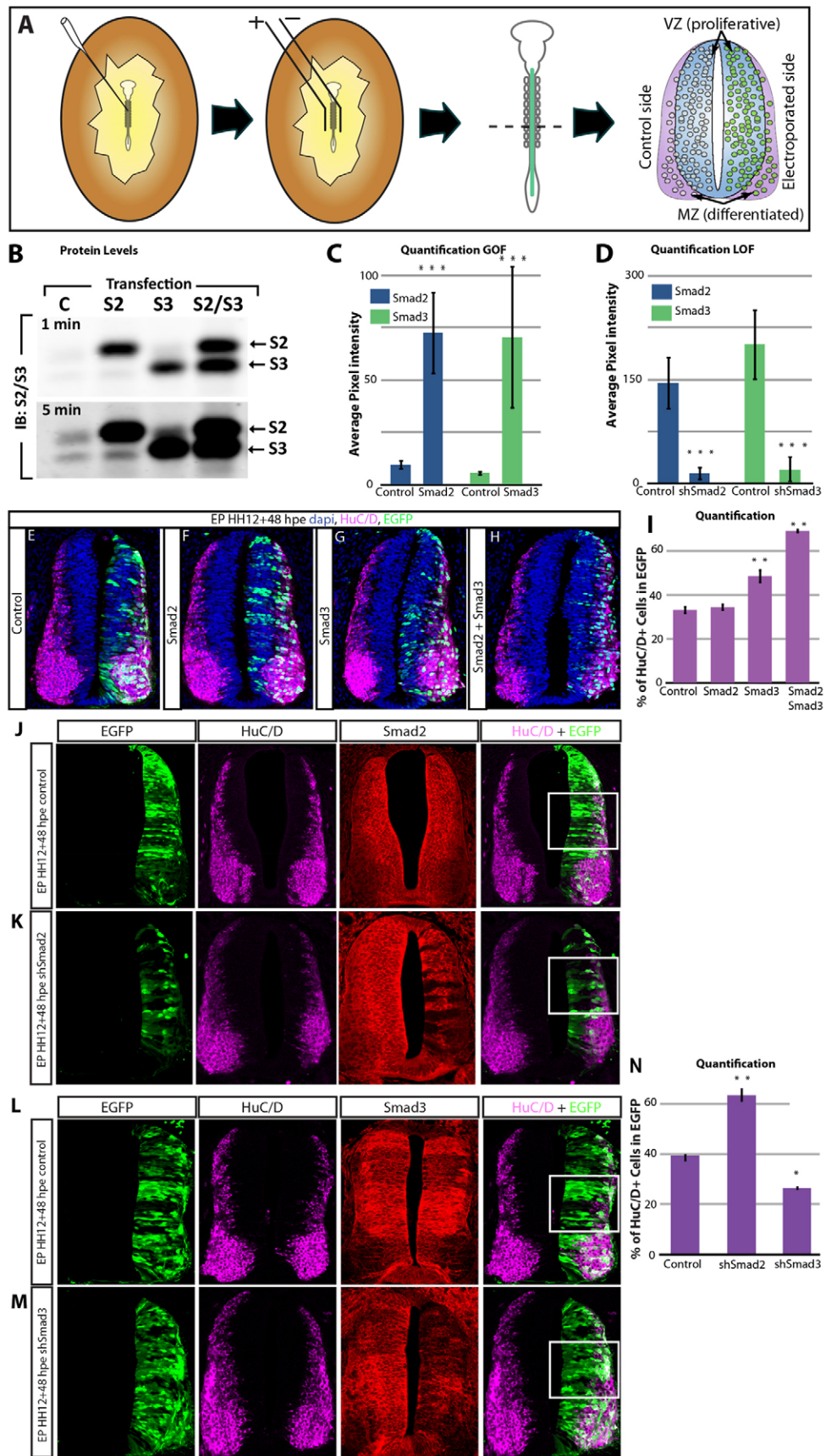


Fig. 2. Smad2 and Smad3 cooperate and antagonize in neurogenesis.

(A) Schematic representation of DNA injection, electroporation and section of transfected chick embryo neural tube. (B) Total protein levels (Smad2 and Smad3) measured by western blot in chick embryo neural tube (C, control) electroporated with Smad2 (S2), Smad3 (S3) or co-electroporated with both Smad2 and Smad3 (S2/S3). (C) Quantification of immunofluorescence intensity in control cells and in cells electroporated with Smad2 and Smad3. (D) Quantification of immunofluorescence intensity in control cells, and cells electroporated with shSmad2 and shSmad3. (E–H) Representative confocal sections after electroporation of indicated DNAs (EGFP⁺ cells), immunostained for the pan-neuronal marker HuC/D (purple) and for DAPI (blue). (I) Quantification of electroporated (EGFP⁺) cells that are differentiated (HuC/D⁺), in each condition. (J–M) Representative confocal sections after electroporation of indicated DNAs (EGFP⁺ cells, green), immunostained for the pan-neuronal marker HuC/D (purple) and for Smad2 (K) or Smad3 (M) (red; boxed areas show the region selected for quantification). (N) Quantification of electroporated (EGFP⁺) cells that are differentiated (HuC/D⁺), in each condition. Error bars represent s.e.m.

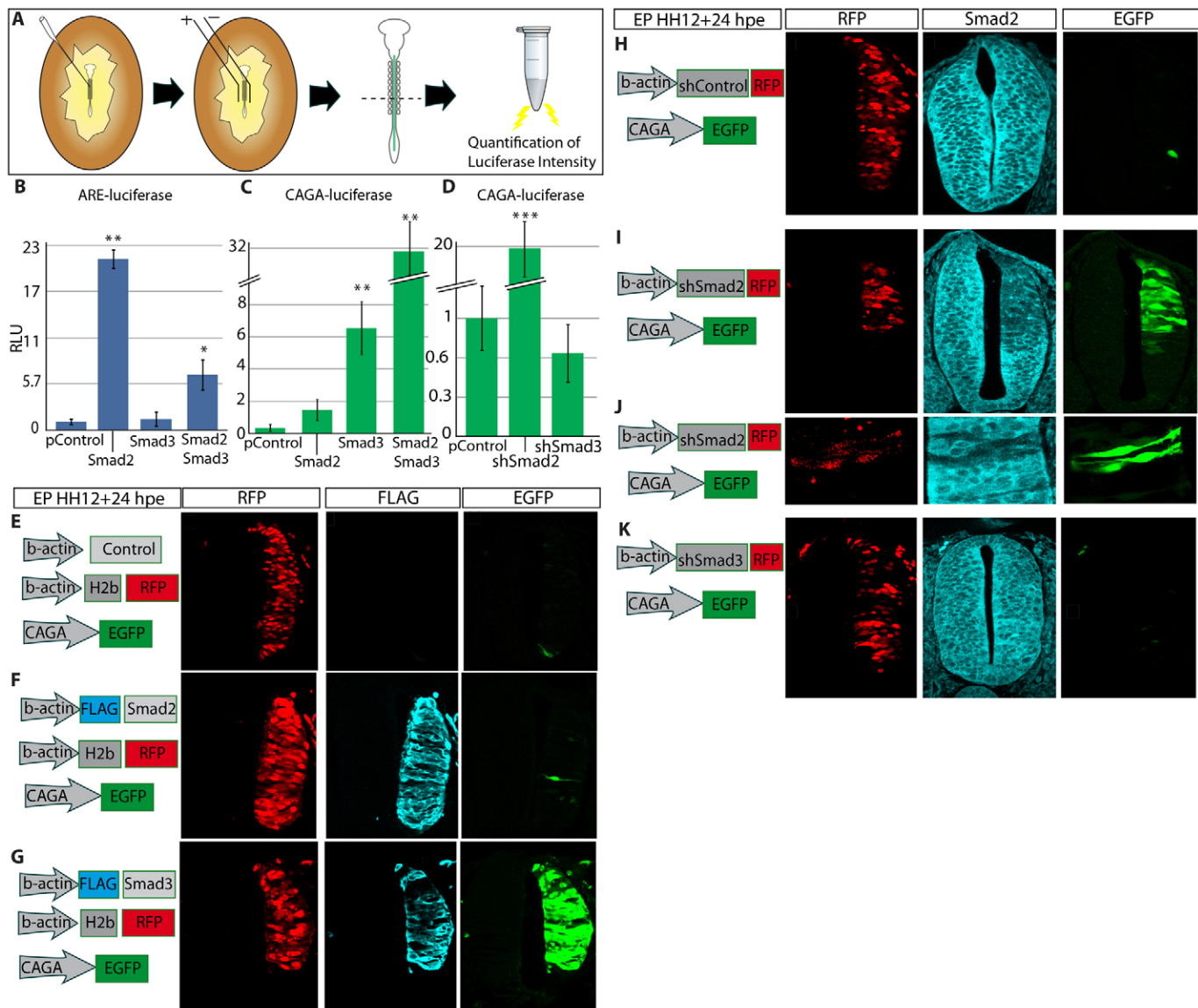


Fig. 3. Smad2 and Smad3 cooperate and antagonize in specific targets of transcription. (A) Schematic representation of DNA injection, electroporation and luciferase assay in transfected chick embryo neural tube. (B) Luciferase activity driven by the Smad2-specific ARE reporter after electroporation of indicated DNAs (concentration of electroporated DNA maintained constant for all experiments). (C,D) Activity of the Smad3-specific CAGA reporter after electroporation of indicated DNAs. Error bars represent s.e.m. (E–G) Representative confocal sections after co-electroporation of the CAGA-EGFP with the indicated DNAs. H2b-RFP (red) is used as electroporation control, FLAG (blue) staining identify the electroporated DNAs, EGFP (green) identify the activated reporter. (H–K) Representative confocal sections after co-electroporation of the CAGA-EGFP with the indicated DNAs. H2b-RFP (red) is used as electroporation control, anti-Smad2 (blue) staining identify endogenous Smad2 expression, EGFP (green) identify the activated reporter.

(Fig. 4A). However, increasing Smad3 ($\sim 12\times$, based on experimental data) enhances transcription of Smad3 ($\sim 3\times$ increase) targets while reducing transcription of specific Smad2 targets ($\sim 7\times$ decrease; Fig. 4A). A simultaneous increase in Smad2 and Smad3 reduces Smad2-specific targets compared with the transcription provoked by Smad2 alone ($\sim 1.2\times$ decrease), whereas it enhances Smad3-specific transcription ($\sim 1.5\times$ increase) compared with Smad3 alone. Moreover, the model predicts that a reduction in Smad2 levels ($\sim 9\times$ decrease) increases Smad3-specific targets ($\sim 3\times$ increase; Fig. 4A, LOF). Together, these *in silico* experiments qualitatively reproduce *in vivo* responses for Smad2- and Smad3-specific target genes (Fig. 4B–D).

Overall, the mathematical model reproduced the experimental data when we consider that Smad4 is not limiting for the formation of the heterotrimers, and that the transcriptional trimers are formed reflecting the concentration of Smad2 and Smad3. In the wild-type state, R-Smad proteins interact with one another and with Smad4 to form each type of possible heterotrimer (S_{224} , S_{234} and S_{334}). However, Smad2 targets are activated solely by the S_{224} complex, whereas Smad3 targets are activated both by S_{234} and S_{334} . Augmenting the amount of Smad2 favors the formation of S_{224} , and reduces the formation of S_{234} and S_{334} trimers. Conversely, increasing Smad3 favors the formation of the S_{334} , and reduces that of S_{234} and S_{224} complexes. Similarly,

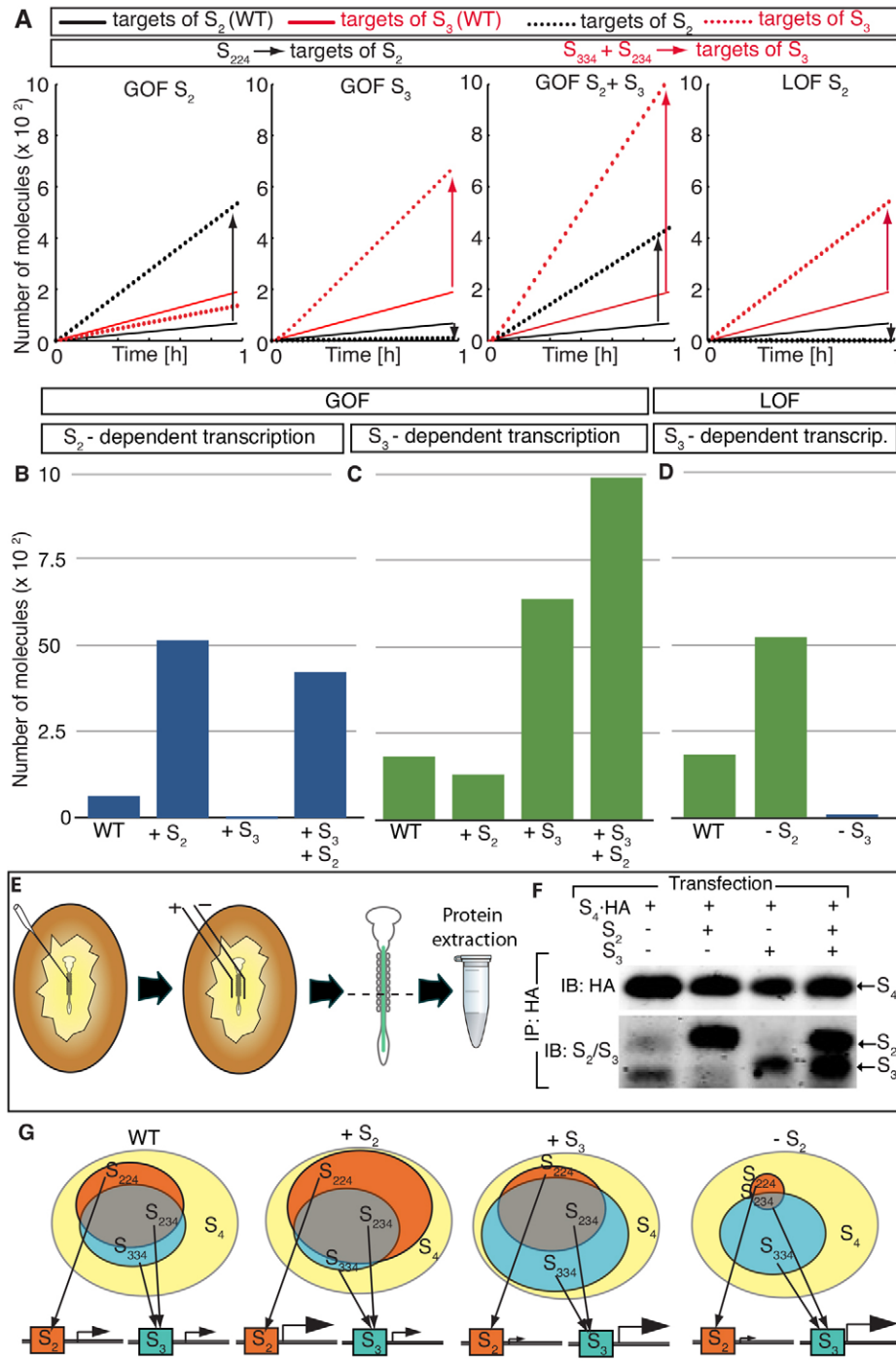


Fig. 4. Numerical model of the pathway predicts the dual antagonism and cooperativity between the R-Smad proteins.

(A) Temporal evolution of transcription of Smad2 (S₂)-specific targets (black dotted line) and Smad3 (S₃)-specific targets (red dotted line) after gain-of-function (GOF) and loss-of-function (LOF). Wild-type time evolution corresponds to the solid black line (S₂-specific targets) and solid red line (S₃-specific targets). (B–D) Bar diagrams of maximum activation levels obtained by the *in silico* model, to be compared with the experimental data shown in Fig. 3B–D. (E) Schematic representation of DNA injection, electroporation and protein extraction for co-immunoprecipitation. (F) Co-immunoprecipitation of Smad2, Smad3 and Smad4. In the wild-type condition, the chick embryo neural tube contains the S₂₃₄ trimer. Smad2 electroporation increases the S₂₂₄ trimer, Smad3 electroporation increases S₃₃₄ trimer, co-electroporation of Smad2 and Smad3 results in the formation of the S₂₃₄ trimer. Smad4 (HA) is constant. (G) Schematic model of the formation of transcriptional complexes and regulation of target genes after wild-type conditions, GOF of Smad2, GOF of Smad3 and LOF of Smad2. Size of arrows in promoter illustrate increase or decrease of transcription compared with the wild type.

a reduction in Smad2 would therefore reduce the formation of S₂₂₄, and increase the formation of S₂₃₄ and S₃₃₄, thereby resulting in the activation of Smad3-specific targets and enhanced neurogenesis (Fig. 4B–D).

To experimentally test the outcome of this *in silico* model, we quantified the trimer formation in each experimental condition (Fig. 4E,F). In the wild-type state, the chick embryo neural tube contains the S₂₃₄ trimer (Fig. 4F), whereas when Smad2 is overexpressed, the S₂₂₄ trimer preferentially forms, without affecting the Smad3-specific transcription of neurogenic targets (Fig. 4F,G). Smad3 overexpression results in the preferential

formation of the S₃₃₄ trimer, which enhances Smad3-specific transcription and neurogenesis (Fig. 4F,G). Similarly, co-expression of Smad2 and Smad3 enhances transcription and neurogenesis of Smad3 by promoting the formation of the S₂₃₄ trimer (Fig. 4F,G).

Here we show *in vivo* and *in silico* that the formation of transcriptionally active Smad2/3 hetero-trimers dictates the dynamics of Smad2- and Smad3-specific transcription. Although clearly modulated by Smad2, the role of TGF- β in neurogenesis follows the trend of Smad3 direct targets: it is enhanced after Smad3 GOF alone or in combination with Smad2, diminished after Smad3 LOF and increased after Smad2 LOF.

This correlates with the binding of Smad3, but not Smad2, to the stress response factor ATF3 in response to TGF- β , which mediates the repression of transcription of *Id1* (inhibitor of DNA binding 1) (Kang et al., 2003). Additional direct targets controlling proliferation and differentiation might include p21CIP1 and p15INK4b, because their regulatory regions have binding sites for Smad3 (Gomis et al., 2006).

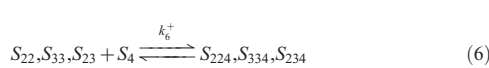
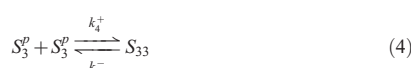
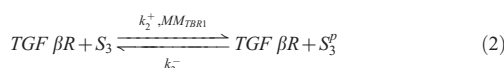
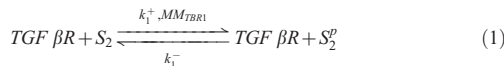
Our model predicts an increase in Smad2-driven transcription after Smad3 LOF, which we could not detect in our *in vivo* experiments owing to the poor sensitivity of the ARE-luciferase reporter. This prediction is consistent with the results in tissue culture experiments where the activity of the ARE reporter is reduced in Smad2-null cells, whereas it is activated in Smad3-null cells (Piek et al., 2001). It also fits the data showing that TLP, a TRAP-1-like protein that does not phosphorylate R-Smad proteins, represses the ability of Smad3 to form a transcriptionally active complex while increasing Smad2-driven transcription (Felici et al., 2003).

We propose that the mechanism reported in this study is responsible for the divergence between studies that focused on comparing the functions of Smad2 and Smad3 in other biological contexts. Indeed, this dual co-operation/antagonism not only influences neurogenesis but also affects other biological events regulated by the TGF- β pathway. A deeper understanding of how R-Smad proteins interact will be crucial to understand the dynamics and function of the TGF- β pathway in order to develop more efficient treatments for diseases in which this pathway is compromised, because impairment of the growth inhibitory function of TGF- β is considered to be a hallmark of cancer (Dennler et al., 1999; Hanahan and Weinberg, 2000).

Materials and Methods

Mathematical model

The models consist of a set of ordinary differential equations solved numerically using a Matlab script developed in-house (The Mathworks[®], Natick, MA), and based on the following interactions (code available upon request):



TGF β R, S_2 and S_3 correspond to concentrations of the active receptor complex and unphosphorylated Smad2 and Smad3 respectively. Equations 3–5 account for binding of the phosphorylated R-Smad proteins S_2^p and S_3^p to form homodimers S_{22} , S_{33} , and heterodimers S_{23} . These complexes bind via Eq. 6 to Smad4 (S_4), forming the three possible heterotrimers S_{224} , S_{334} , S_{234} that can potentially enter the nuclei and bind to specific regulatory sequences to regulate transcription regulated by Smad2 and Smad3-specific binding sites.



Eqs. 7 and 9 account for the transcription of the targets of S_2 and S_3 activated by the S_{224} and S_{334} complex, respectively. There is no experimental evidence of how the heterotrimer S_{234} regulates S_2 - or S_3 -specific transcription, but our experimental data (Fig. 3C) show strong activation of the S_3 -specific CAGA sequence when Smad2 and Smad3 are co-electroporated, suggesting a role of S_{234} in S_3 -specific transcription. This is introduced in the model via Eq. 8.

We consider a Michaelis–Menten type of interaction for the phosphorylation of the R-Smad proteins (Eqs. 1,2). Michaelis–Menten constants and phosphorylation rates of each of the R-Smad proteins by the TGF β R receptor were chosen to be equal. Transcription was computed as a Hill function of the amount of active complex with no cooperativity. Parameter values (supplementary material Table S1) and parameter selection are discussed in detail in the selection of model parameters section.

Several authors (e.g. Labbé et al., 1998) hypothesize that the antagonism emerges from competition of the R-Smad proteins to bind to Smad4, but the fact that the pathway can get activated up to 20 times above the endogenous levels (Fig. 3C,D) reflects that the amount of Smad4 is not the limiting reactant in the reaction in the wild-type situation. In addition, this hypothesis does not explain the strong cooperativity in Smad3 direct targets when combining Smad2 with Smad3, explained by our model.

The differential equations derived from this model are as follows:

$$\frac{dS_2}{dt} = k_1^- \cdot S_2^p - \frac{k_1^+ \cdot TGF\beta R \cdot S_2}{S_2 + MM_{TBR1}} \quad (10)$$

$$\frac{dS_3}{dt} = k_2^- \cdot S_3^p - \frac{k_2^+ \cdot TGF\beta R \cdot S_3}{S_3 + MM_{TBR1}} \quad (11)$$

$$\frac{dS_2^p}{dt} = \frac{k_1^+ \cdot TGF\beta R \cdot S_2}{S_2 + MM_{TBR1}} - k_1^- \cdot S_2^p - 2k_3^+ \cdot (S_2^p)^2 + 2k_3^- \cdot S_{22} - k_5^+ \cdot S_2^p \cdot S_3^p + k_5^- \cdot S_{23} \quad (12)$$

$$\frac{dS_3^p}{dt} = \frac{k_2^+ \cdot TGF\beta R \cdot S_3}{S_3 + MM_{TBR1}} - k_2^- \cdot S_3^p - 2k_4^+ \cdot (S_3^p)^2 + 2k_4^- \cdot S_{33} - k_5^+ \cdot S_2^p \cdot S_3^p + k_5^- \cdot S_{23} \quad (13)$$

$$\frac{dS_{22}}{dt} = k_3^+ \cdot (S_2^p)^2 - k_3^- \cdot S_{22} - k_6^+ \cdot S_{22} \cdot S_4 + k_6^- \cdot S_{224} \quad (14)$$

$$\frac{dS_{33}}{dt} = k_4^+ \cdot (S_3^p)^2 - k_4^- \cdot S_{33} - k_6^+ \cdot S_{33} \cdot S_4 + k_6^- \cdot S_{334} \quad (15)$$

$$\frac{dS_{23}}{dt} = k_5^+ \cdot S_2^p \cdot S_3^p + k_5^- \cdot S_{23} - k_6^+ \cdot S_{23} \cdot S_4 + k_6^- \cdot S_{234} \quad (16)$$

$$\frac{dS_{224}}{dt} = k_6^+ \cdot S_{22} \cdot S_4 - k_6^- \cdot S_{224} \quad (17)$$

$$\frac{dS_{334}}{dt} = k_6^+ \cdot S_{33} \cdot S_4 - k_6^- \cdot S_{334} \quad (18)$$

$$\frac{dS_{234}}{dt} = k_6^+ \cdot S_{23} \cdot S_4 - k_6^- \cdot S_{234} \quad (19)$$

$$\frac{\text{targets of } S_2}{dt} = \frac{k_7^+ \cdot S_{224}}{MM_S + S_{224}} \quad (20)$$

$$\frac{\text{targets of } S_3}{dt} = \frac{k_7^+ \cdot S_{234}}{MM_S + S_{234}} + \frac{k_8^+ \cdot S_{334}}{MM_S + S_{334}} \quad (21)$$

Selection of model parameters

Concentration and activity of $[S_2]^{t=0}$, $[S_3]^{t=0}$ and $[S_4]^{t=0}$

Experimental measurements of total concentration of Smad2, Smad3 and Smad4 have been performed in a specific cell type (Clarke et al., 2006), reporting values of 100,000, 20,000 and 100,000 total molecules per cell of Smad2, Smad3 and Smad4, respectively. Assuming a cell volume of 1×10^{-12} l, this gives us a value of

$[S_2]_{WT}^{t=0}=166$ nM, $[S_3]_{WT}^{t=0}=33$ nM, $[S_4]_{WT}^{t=0}=166$ nM. Because wild-type values of Smad2, Smad3 and Smad4 are likely to be very cell-type dependent, and our three semi-quantitative estimations (immunofluorescence, western blot and co-immunoprecipitation) reflect similar values for Smad2 and Smad3, we decided to use for the model a standard value of 100 nM for all three Smad proteins, which is close to the experimental measurements reported previously (Clarke et al., 2006). Our model predictions are robust against slight changes in Smad concentration (within the same order of magnitude), and it also works when using the exact values measured previously (Clarke et al., 2006).

To estimate the concentration after GOF, we performed experiments where we electroporated Smad2 and Smad3 and immunostained neural tube sections 24 hpe (supplementary material Fig. S3). This way, we can measure the change in immunofluorescence intensity between not electroporated and electroporated cells. The average increase in pixel intensity for Smad2 was $7.6\times$, and for Smad3 was $12.1\times$. This gives us a final values for $[S_2]_{GOF}^{t=0}=1216$ nM, $[S_3]_{GOF}^{t=0}=403$ nM. Quantification of this experiment is shown in Fig. 2H.

To estimate the concentration after LOF, we performed measurements of the immunofluorescence intensity in cells electroporated with shRNA against Smad2 and Smad3 compared with control (supplementary material Fig. S3). The average reduction in pixel intensity for Smad2 was $9.6\times$, and for Smad3 was $10.1\times$. This gives us a final values of $[S_2]_{LOF}^{t=0}=17.4$ nM, $[S_3]_{LOF}^{t=0}=3.3$ nM. Quantification of this experiment is shown in Fig. 2I.

The balance between phosphorylation and de-phosphorylation of the R-Smad proteins has been shown to be a key mechanism to regulate the dynamics of nuclear–cytoplasmic shuttling (Hill, 2009), so nuclear localization of the R-Smad proteins can be used as a readout of the pathway activity. This way, the balance between phosphorylation and de-phosphorylation in our model in conditions of pathway activation, should mimic the experimental (i.e. most R-Smad phosphorylated after pathway activation, and most R-Smad un-phosphorylated when the pathway is inactive). Owing to the lack of experimental data regarding the un-phosphorylation rate of R-Smad, for our model we use a standard value used in generalized models involving phosphatase activity (Khodolenko et al., 2000; Lipkow and Odde, 2008) and other models of $k_1^-, k_2^- = 1 \text{ s}^{-1}$.

Concentration and activity of TGF β R

Previous experimental data (Wakefield et al., 1987) and other previous TGF β R models (Zi et al., 2011) use a value of total $TGF\beta R-R-I=1000$. Our model does not take into account receptor complex assembly and multimerization of receptor subtypes (Clarke and Liu, 2008), so we assume 20% of these values of total $[TGF\beta R-TypeI-R]$ as active after ligand stimulation. Because these are membrane proteins, to calculate the concentration, we assume that they are distributed in a volume equal to the cell area (given a cell radius value of $13 \mu\text{m}$ for a spherical cell volume of $1 \times 10^{-12} \text{ l}$) times the typical height of a ligand–receptor complex (Allard et al., 2012) to obtain a value for $[TGF\beta]=149$ nM.

For the value of k_1^+, k_2^+ , we used the median value used previously (Clarke et al., 2006). The value for the Michaelis–Menten constant has been selected within the range listed (Clarke et al., 2006) (the median 2.89×10^5 molecules resulted in very low values of R-Smad phosphorylation, so for lack of experimental data we assume the minimum value listed (Clarke et al., 2006) of $MM_{TGF\beta R}=633$ molecules = 1.03 nM. Values around ten times above or below the selected value also produce simulation results in agreement with our experimental data.

Association and dissociation rates of R-Smad proteins

Due to lack of experimental values for association and dissociation of the R-Smad proteins after phosphorylation, we have used values where after phosphorylation, steady state is achieved in the order of seconds, and most of the R-Smad proteins are in a dimer and trimer configuration when phosphorylated, as shown experimentally. Experiments in Fig. 3C,D show that removing Smad2 increases activation of Smad3-specific targets, suggesting that the presence of Smad2 prevents Smad3 from activating its own targets. To take this into account, Smad3 affinity towards Smad3 was set lower than towards Smad2. This configuration induces more Smad2–Smad3 than Smad3–Smad3 complexes.

DNA regulation by the R-Smad heterotrimers

To our knowledge, experimental measurements of transcription rates of the different heterotrimer complexes in specific targets for Smad2 and Smad3, have not been reported. Previous systematic studies on mRNA production (Schwahnässer et al., 2011) have shown an average of 10 mRNA molecules per hour. In addition, the same studies have reported an average of 140 protein molecules per mRNA. So values for $k_7^+=0.38 \text{ s}^{-1}$ was chosen based on these data.

Fig. 3C shows that Smad2, when co-electroporated with Smad3, plays a role in Smad3 transcription. Our model fits the experimental data when considering that this role of the Smad2–Smad3–Smad4 complex in Smad3-specific targets is lower than the role of the Smad3–Smad3–Smad4 complex, so we set $k_8^+=19 \text{ s}^{-1}$ generically as $50\times$ higher than k_7^+ . Differences between k_8^+ and k_7^+ above $25\times$ also reproduce the experimental data. Values higher than $50\times$ difference result in higher differences between the different conditions, also in agreement with the

experimental data, where fold change in transcription compared with the wild type is qualitatively higher than the model prediction.

Plasmids

Non-overlapping sequences of chicken *Smad3* (bp 550–569) and *Smad2* (bp 264–283) were targeted following a previously published protocol. These fragments were cloned into the pSHIN vector (Kojima et al., 2004) to generate short hairpin RNAs (shRNAs) that could be electroporated into the neural tube. Controls were performed by electroporating the empty pSHIN vector. Human N-terminal FLAG-tagged Smad2, Smad3 and Smad4 were cloned into a pCIG vector.

In ovo electroporation

Chick embryos were staged according to Hamburger and Hamilton (Hamburger and Hamilton, 1951). Plasmid DNA was injected into the lumen of HH stage 12 neural tubes, electrodes were placed either side of the neural tube and electroporation was performed using an Intracel Dual Pulse (TSS-100) electroporator delivering 50 ms square pulses of 40 V. Transfected embryos were allowed to develop for 24–48 hours, dissected and processed for immunohistochemistry, *in situ* hybridization, luciferase assays or protein extraction.

Immunohistochemistry and in situ hybridization

For *in situ* hybridization, embryos were fixed overnight at 4°C in 4% paraformaldehyde diluted in PBS, rinsed and processed for whole-mount RNA *in situ* hybridization using probes against chick Smad2 and Smad3 from the chicken EST project following standard procedures. Immunofluorescence was performed on transverse sections ($40 \mu\text{m}$) after fixation in 4% paraformaldehyde diluted in PBS for 2–4 hours at 4°C using the following monoclonal antibodies: Smad2 (Cell Signaling, 5339), Smad3 (Abcam, ab28379), HuC/D (Molecular Probes, A-21271). Anti-HA and anti-FLAG antibodies were generated in-house (Sebastian Pons Laboratory).

In vivo luciferase-reporter assay

Embryos were electroporated with the DNAs indicated with a firefly-luciferase reporter construct driven by the ARE and CAGA promoter sequences, and a Renilla luciferase reporter construct for normalization (Promega). Embryos were harvested after 24 hours *in ovo* and only the interlimb sections of GFP-positive neural tubes were dissected and homogenized on ice with a Dounce homogenizer in passive lysis buffer. Firefly and Renilla luciferase activities were measured using a dual luciferase reporter assay system (Promega).

Immunoprecipitation and western blotting

For the study of the S234 complexes by co-immunoprecipitation, embryos were co-electroporated at HH14 with the DNAs indicated (the total amount of DNA electroporated was normalized with the empty vector pCIG, $n=5$ per condition) and the neural tube was dissected at 24 hpe. The cells were lysed by sonication pulses in lysis buffer (20 mM Tris-HCl, pH 7.4, 137 mM NaCl, 10% glycerol, 1% NP-40, 1 mM CaCl₂, 1 mM MgCl₂, 0.05% sodium azide) supplemented with protease inhibitors (1 mM PMSF, 1 $\mu\text{g}/\text{ml}$ aprotinin and 1 $\mu\text{g}/\text{ml}$ leupeptin, Sigma). The insoluble material was removed by centrifugation and one tenth of the resulting supernatant was reserved as the input material; the remaining volume was immunoprecipitated for 4 hours at 4°C with a monoclonal anti-HA agarose conjugate (Sigma). The beads were washed three times and boiled with 2× SDS loading buffer and the samples were resolved by 8% SDS-PAGE. After western blotting, the membranes were incubated with the indicated primary antibodies and infra-red-tagged secondary antibodies (anti-Rabbit IgG DyLight 800 conjugate and anti-rabbit IgG DyLight 680 conjugate; Thermo). The membranes were scanned using the Odyssey infrared imager (Li-Cor).

Quantification and data analysis

The ratio of differentiated electroporated cells was calculated by first quantifying the number of EGFP⁺ cells and then by quantifying the HuC/D⁺ cells among those that were electroporated. At least ten different confocal transversal sections of the neural tube were quantified from at least three different electroporated embryos. The change in immunofluorescence staining intensity was quantified in 50 electroporated cells versus 50 non-electroporated cells in three different neural tube sections for each condition (supplementary material Fig. S3). The bars represent the mean value and the error bars represent the s.e.m. Statistical significance in terms of *P*-values was calculated using the Z-test function in Numbers (Macintosh).

Acknowledgements

We are grateful to Susana Usieto for her invaluable technical assistance.

Author contributions

D.G.M. and E.M. conceived and performed the experiments, analysed the results and wrote the manuscript. E.G.G. and S.P. conceived, performed and analysed the WB and co-IP experiments.

Funding

D.G.M. holds a RYC-2010-07450 position. This work was supported by the Spanish Government [grant numbers BFU2011-30303 to D.G.M.; BFU2010-18959 to E.M.; BFU2011-24099 to S.P.] and a Marie Curie International Reintegration Grant from the EC [grant number 248346-NMSSBLS to D.G.M.].

Supplementary material available online at
<http://jcs.biologists.org/lookup/suppl/doi:10.1242/jcs.130435/-DC1>

References

- Allard, J. F., Dushek, O., Coombs, D. and van der Merwe, P. A. (2012). Mechanical modulation of receptor-ligand interactions at cell-cell interfaces. *Biophys. J.* **102**, 1265-1273.
- Bernard, D. J. (2004). Both SMAD2 and SMAD3 mediate activin-stimulated expression of the follicle-stimulating hormone beta subunit in mouse gonadotrope cells. *Mol. Endocrinol.* **18**, 606-623.
- Brown, K. A., Pietenpol, J. A. and Moses, H. L. (2007). A tale of two proteins: differential roles and regulation of Smad2 and Smad3 in TGF-beta signaling. *J. Cell. Biochem.* **101**, 9-33.
- Cellière, G., Fengos, G., Hervé, M. and Iber, D. (2011). Plasticity of TGF- β signaling. *BMC Syst. Biol.* **5**, 184.
- Chen, X., Rubock, M. J. and Whitman, M. (1996). A transcriptional partner for MAD proteins in TGF-beta signalling. *Nature* **383**, 691-696.
- Clarke, D. C. and Liu, X. (2008). Decoding the quantitative nature of TGF-beta/Smad signaling. *Trends Cell Biol.* **18**, 430-442.
- Clarke, D. C., Betterton, M. D. and Liu, X. (2006). Systems theory of Smad signalling. *Syst. Biol.* **153**, 412-424.
- Dennler, S., Itoh, S., Vivien, D., ten Dijke, P., Huet, S. and Gauthier, J. M. (1998). Direct binding of Smad3 and Smad4 to critical TGF beta-inducible elements in the promoter of human plasminogen activator inhibitor-type 1 gene. *EMBO J.* **17**, 3091-3100.
- Dennler, S., Huet, S. and Gauthier, J. M. (1999). A short amino-acid sequence in MH1 domain is responsible for functional differences between Smad2 and Smad3. *Oncogene* **18**, 1643-1648.
- Dunn, N. R., Koonce, C. H., Anderson, D. C., Islam, A., Bikoff, E. K. and Robertson, E. J. (2005). Mice exclusively expressing the short isoform of Smad2 develop normally and are viable and fertile. *Genes Dev.* **19**, 152-163.
- Felici, A., Wurthner, J. U., Parks, W. T., Giam, L. R., Reiss, M., Karpova, T. S., McNally, J. G. and Roberts, A. B. (2003). TLP, a novel modulator of TGF-beta signaling, has opposite effects on Smad2- and Smad3-dependent signaling. *EMBO J.* **22**, 4465-4477.
- García-Campmany, L. and Martí, E. (2007). The TGFbeta intracellular effector Smad3 regulates neuronal differentiation and cell fate specification in the developing spinal cord. *Development* **134**, 65-75.
- Gomis, R. R., Alarcón, C., Nadal, C., Van Poznak, C. and Massagué, J. (2006). C/EBPbeta at the core of the TGFbeta cytostatic response and its evasion in metastatic breast cancer cells. *Cancer Cell* **10**, 203-214.
- Hamburger, V. and Hamilton, H. L. (1951). A series of normal stages in the development of the chick embryo. *J. Morphol.* **88**, 49-92.
- Hanahan, D. and Weinberg, R. A. (2000). The hallmarks of cancer. *Cell* **100**, 57-70.
- Hill, C. S. (2009). Nucleocytoplasmic shuttling of Smad proteins. *Cell Res.* **19**, 36-46.
- Jia, S., Ren, Z., Li, X., Zheng, Y. and Meng, A. (2008). smad2 and smad3 are required for mesendoderm induction by transforming growth factor-beta/nodal signals in zebrafish. *J. Biol. Chem.* **283**, 2418-2426.
- Kang, Y., Chen, C. R. and Massagué, J. (2003). A self-enabling TGFbeta response coupled to stress signaling: Smad engages stress response factor ATF3 for Id1 repression in epithelial cells. *Mol. Cell* **11**, 915-926.
- Khodatako, B. N., Brown, G. C. and Hoek, J. B. (2000). Diffusion control of protein phosphorylation in signal transduction pathways. *Biochem. J.* **350**, 901-907.
- Kojima, S. i., Vignjević, D. and Borisy, G. G. (2004). Improved silencing vector co-expressing GFP and small hairpin RNA. *Biotechniques* **36**, 74-79.
- Labbé, E., Silvestri, C., Hoodless, P. A., Wrana, J. L. and Attisano, L. (1998). Smad2 and Smad3 positively and negatively regulate TGF beta-dependent transcription through the forkhead DNA-binding protein FAST2. *Mol. Cell* **2**, 109-120.
- Li, Q., Pangas, S. A., Jorgez, C. J., Graff, J. M., Weinstein, M. and Matzuk, M. M. (2008). Redundant roles of SMAD2 and SMAD3 in ovarian granulosa cells in vivo. *Mol. Cell. Biol.* **28**, 7001-7011.
- Lipkow, K. and Odde, D. J. (2008). Model for protein concentration gradients in the cytoplasm. *Cell. Mol. Bioeng.* **1**, 84-92.
- Massagué, J. (2000). How cells read TGF-beta signals. *Nat. Rev. Mol. Cell Biol.* **1**, 169-178.
- Melke, P., Jönsson, H., Pardali, E., ten Dijke, P. and Peterson, C. (2006). A rate equation approach to elucidate the kinetics and robustness of the TGF-beta pathway. *Biophys. J.* **91**, 4368-4380.
- Moustakas, A. and Heldin, C. H. (2002). From mono- to oligo-Smads: the heart of the matter in TGF-beta signal transduction. *Genes Dev.* **16**, 1867-1871.
- Moustakas, A., Souchelnytskyi, S. and Heldin, C. H. (2001). Smad regulation in TGF-beta signal transduction. *J. Cell Sci.* **114**, 4359-4369.
- Petersen, M., Pardali, E., van der Horst, G., Cheung, H., van den Hoogen, C., van der Pluijm, G. and Ten Dijke, P. (2010). Smad2 and Smad3 have opposing roles in breast cancer bone metastasis by differentially affecting tumor angiogenesis. *Oncogene* **29**, 1351-1361.
- Piek, E., Ju, W. J., Heyer, J., Escalante-Alcalde, D., Stewart, C. L., Weinstein, M., Deng, C., Kucherlapati, R., Bottinger, E. P. and Roberts, A. B. (2001). Functional characterization of transforming growth factor beta signaling in Smad2- and Smad3-deficient fibroblasts. *J. Biol. Chem.* **276**, 19945-19953.
- Schmierer, B., Tournier, A. L., Bates, P. A. and Hill, C. S. (2008). Mathematical modeling identifies Smad nucleocytoplasmic shuttling as a dynamic signal-interpreting system. *Proc. Natl. Acad. Sci. USA* **105**, 6608-6613.
- Schwanhäußer, B., Busse, D., Li, N., Dittmar, G., Schuchhardt, J., Wolf, J., Chen, W. and Selbach, M. (2011). Global quantification of mammalian gene expression control. *Nature* **473**, 337-342.
- Shi, Y. and Massagué, J. (2003). Mechanisms of TGF-beta signaling from cell membrane to the nucleus. *Cell* **113**, 685-700.
- ten Dijke, P. and Hill, C. S. (2004). New insights into TGF-beta-Smad signalling. *Trends Biochem. Sci.* **29**, 265-273.
- Ungefroren, H., Groth, S., Sebens, S., Lehnert, H., Gieseler, F. and Fändrich, F. (2011). Differential roles of Smad2 and Smad3 in the regulation of TGF- β 1-mediated growth inhibition and cell migration in pancreatic ductal adenocarcinoma cells: control by Rac1. *Mol. Cancer* **10**, 67.
- Vilar, J. M. G., Jansen, R. and Sander, C. (2006). Signal processing in the TGF-beta superfamily ligand-receptor network. *PLOS Comput. Biol.* **2**, e3.
- Wakefield, L. M., Smith, D. M., Masui, T., Harris, C. C. and Sporn, M. B. (1987). Distribution and modulation of the cellular receptor for transforming growth factor-beta. *J. Cell Biol.* **105**, 965-975.
- Xie, Z., Chen, Y., Li, Z., Bai, G., Zhu, Y., Yan, R., Tan, F., Chen, Y. G., Guillemot, F., Li, L. et al. (2011). Smad6 promotes neuronal differentiation in the intermediate zone of the dorsal neural tube by inhibition of the Wnt/beta-catenin pathway. *Proc. Natl. Acad. Sci. USA* **108**, 12119-12124.
- Yang, Y. C., Piek, E., Zavadil, J., Liang, D., Xie, D., Heyer, J., Pavlidis, P., Kucherlapati, R., Roberts, A. B. and Böttiger, E. P. (2003). Hierarchical model of gene regulation by transforming growth factor beta. *Proc. Natl. Acad. Sci. USA* **100**, 10269-10274.
- Zi, Z. and Klipp, E. (2007). Constraint-based modeling and kinetic analysis of the Smad dependent TGF-beta signaling pathway. *PLoS ONE* **2**, e936.
- Zi, Z., Feng, Z., Chapnick, D. A., Dahl, M., Deng, D., Klipp, E., Moustakas, A. and Liu, X. (2011). Quantitative analysis of transient and sustained transforming growth factor- β signaling dynamics. *Mol. Syst. Biol.* **7**, 492.

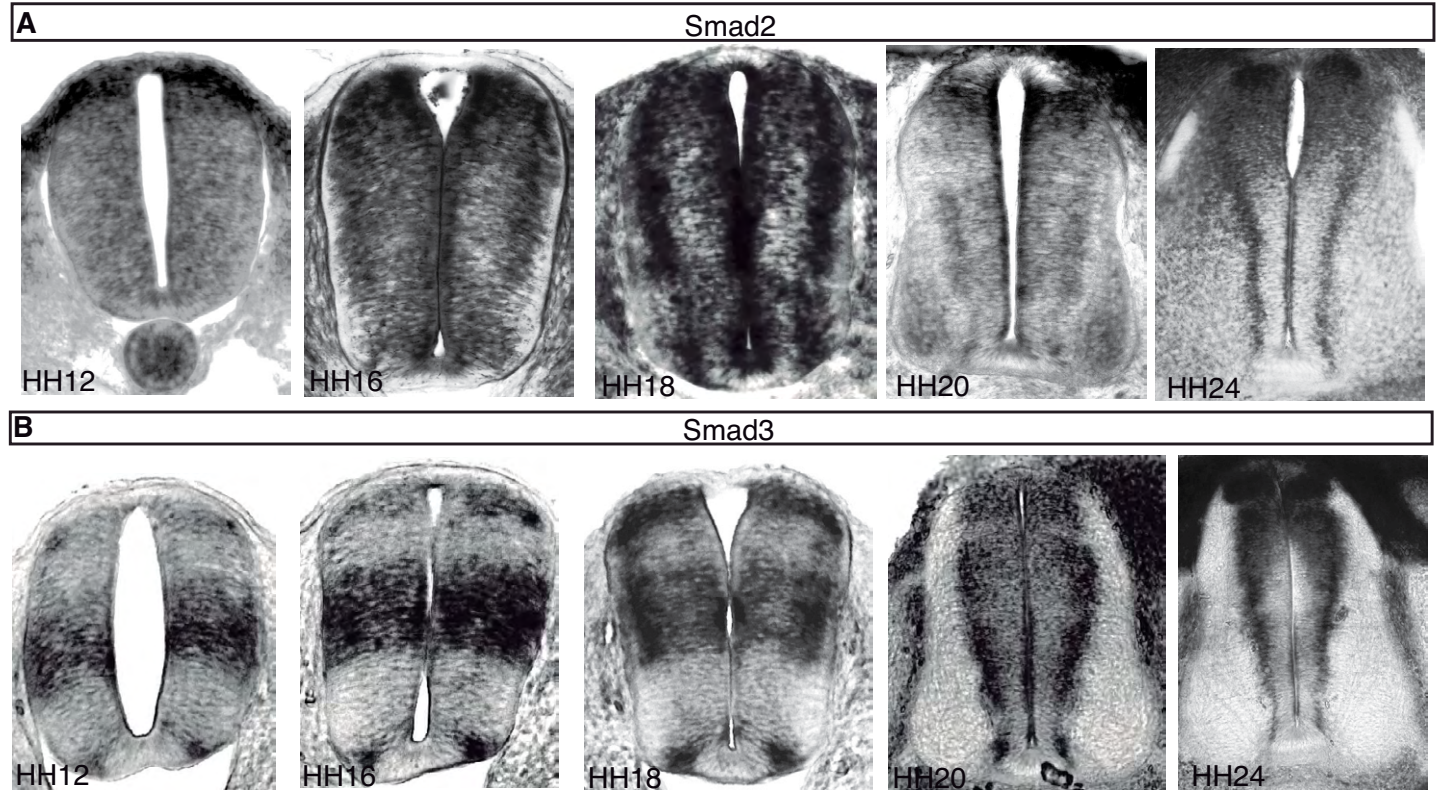


Fig. S1. Smad2 and Smad3 mRNA expression. In-situ hybridization using a Smad2 and Smad3 specific probes at the indicated developmental stages. (A) Smad2 is expressed in the ventricular zone with increased expression at the transition zone at later stages. (B) Smad3 is expressed at the intermediate NT in early stages. Three different regions of high Smad3 expression appear at later stages, as well as increased expression at the transition zone.

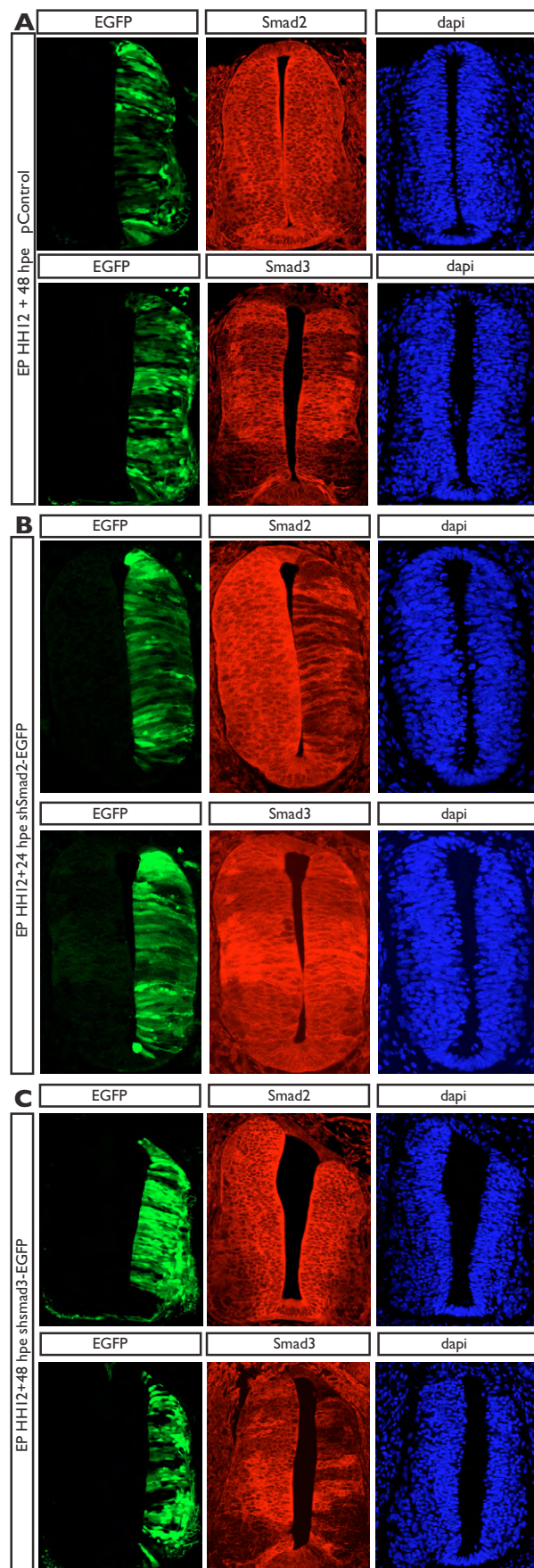


Fig. S2. shSmad2 and shSmad3 strongly reduce expression of their specific targets, without affecting the expression levels of the other R-Smad. (A) Electroporation of control, (B) Electroporation of shSmad2 showing strong reduction in Smad2 electroporated cells, while Smad3 levels remain unchanged. (C) Electroporation of shSmad3 showing strong reduction of Smad3 in electroporated cells, while Smad2 levels remain unchanged. Average pixel intensity measured 48 hpe are shown in Fig. 2I.

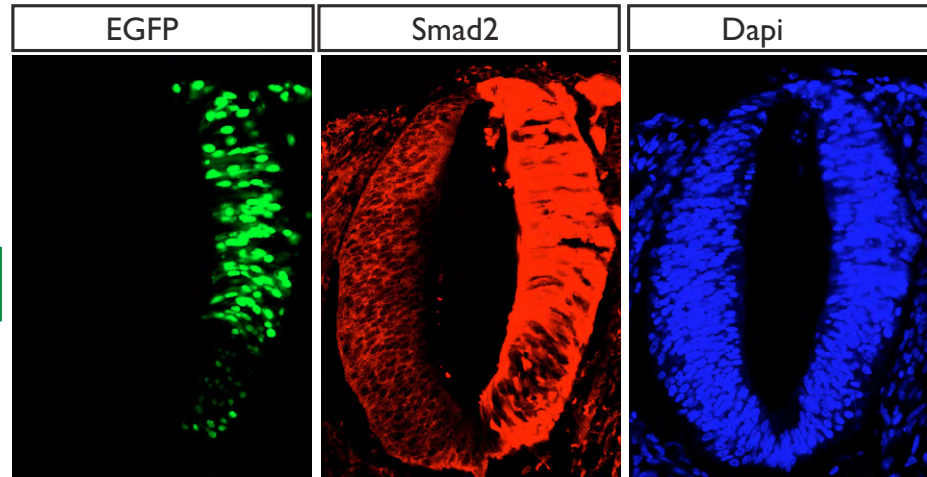
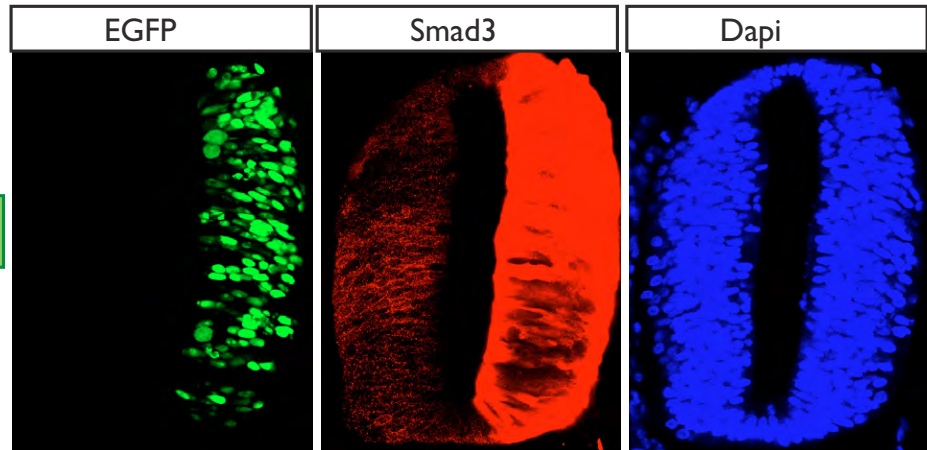
A**B**

Fig. S3. Changes in Smad2 and Smad3 expression after gain-of-function experiments. (A) Immunofluorescence staining of Smad2 after electroporation of Smad2. (B) Immunofluorescence staining of Smad3 after electroporation of Smad3. Average pixel intensity measured 48 hpe are shown in Fig. 2H.

Table S1. Parameters for the Numerical Model

Parameter	Value	Units
t_{max}	60	min
$[TGF\beta R]$	149	nM
$MM_{TGF\beta R}$	1.03	nM
$[S_2]_{WT}^{t=0}$	100	nM
$[S_3]_{WT}^{t=0}$	100	nM
$[S_4]_{WT}^{t=0}$	100	nM
$[S_2]_{GOF}^{t=0}$	1216	nM
$[S_3]_{GOF}^{t=0}$	403	nM
$[S_2]_{LOF}^{t=0}$	17.4	nM
$[S_3]_{LOF}^{t=0}$	3.3	nM
k_1^+, k_2^+	3.5	s^{-1}
MM_S	1.03	nM
k_1^-, k_2^-	1	s^{-1}
k_3^+, k_4^+	0.1	$\text{nM}^{-1}s^{-1}$
k_3^-, k_4^-	1	s^{-1}
$k_5^+,$	1	$\text{nM}^{-1}s^{-1}$
k_5^-	0.1	s^{-1}
k_7^+	0.38	s^{-1}
k_8^+	19	s^{-1}